This is a preprint, the final version is subject to change, of the American Mineralogist (MSA)
Cite as Authors (Year) Title. American Mineralogist, in press.
(DOI will not work until issue is live.) DOI: http://dx.doi.org/10.2138/am.2013.4247

Revised to: American Mineralogist August 31, 2012

Hydrogen isotope fractionation between coexisting hydrous melt and silicate-saturated aqueous fluid: An experimental study *in-situ* at high pressure and temperature

Bjorn Mysen
Geophysical Laboratory
Carnegie Instn. Washington
5251 Broad Branch Rd., NW
Washington DC 20015

Abstract

Hydrogen isotope fractionation between water-saturated silicate melt and silicate-saturated aqueous fluid has been determined experimentally by using vibrational spectroscopy as the analytical tool. The measurements were conducted *in-situ* with samples at the high temperature and pressure of interest in an externally-heated diamond cell in the 450˚-800˚C and 101-1567 MPa temperature and pressure range, respectively. The starting materials were glass of Na-silicate with Na/Si=0.5 (NS4), an aluminosilicate composition with 10 mol % Al_2O_3 and Na/(Al+Si)=0.5 (NA10), and a 50:50 (by volume) H_2O:D_2O fluid mixture. Platinum metal was used to enhance equilibration rate. Isotopic equilibrium was ascertained by using variable experimental duration at given temperature and pressure.

In the Al-free NS4 system, the enthalpy of the D H equilibrium of fluid is 3.1±0.7 kJ/mol, whereas that of coexisting melt equals 0 within error. For NA10 fluids the ΔH=5.2±0.9 kJ/mol, whereas for coexisting NA10 melt, ΔH is near 0 within error. For the exchange equilibrium between melt and coexisting fluid, $H_2O(melt)+D_2O(fluid)$ $H_2O(fluid)+D_2O(melt)$, the ΔH=4.6±0.7 and 6.5±0.7 kJ/mol for NS4 and NA10 compositions, respectively.

The D/H fractionation between melt and fluid is affected significantly by the positive temperature- and pressure-dependence of silicate solubility and silicate structure in silicate-saturated aqueous fluids. Water in melts is much less important than silicate in aqueous fluid because even at the lowest temperature and pressure conditions studied (450˚C/101 MPa), the water content in the melt is so high (> 4 wt%) that further increase

This is a preprint, the final version is subject to change, of the American Mineralogist (MSA)
Cite as Authors (Year) Title. American Mineralogist, in press.
(DOI will not work until issue is live.) DOI: http://dx.doi.org/10.2138/am.2013.4247

in total water by increasing temperature and pressure does not affect the silicate melt structure significantly. This is because most of the water in this concentration range is dissolved in molecular form.

Introduction

Constraints on formation and evolution of planetary interiors, including mantle fluxes and mantle degassing, rely on experimentally-determined distribution of volatile abundance in and isotope fractionation between minerals, fluid, and melt (e.g., Exley et al., 1987; Kasting et al., 1993; Dixon, 1997). Hydrogen isotope fractionation is often employed for this purpose (e.g., Pineau et al., 1998; Tolsthikin and Marty, 1998; Hauri, 2002).

For D/H fractionation between silicate melt and aqueous fluid, experimental data have been reported in which fluid and melt were separated after an experiment and before chemical and isotopic analysis of these phases individually (e.g., Kuroda et al., 1982; Richet et al., 1986; Dobson et al., 1989; Pineau et al., 1998). These data rely, therefore, on perfect or near-perfect physical separation of fluid from melt after an experiment. The separation can be very difficult in particular in experiments where pressures and temperatures were sufficiently high to result in significant silicate solubility in the aqueous fluid (e. g., deep crustal and upper mantle temperature and pressure conditions – see, for example, Manning, 2004). During temperature quenching and decompression after such high-temperature/-pressure experiments, typically some of the dissolved silicate precipitates from the fluid thus changing fluid chemistry before it is analyzed (e.g., Kuroda et al., 1982; Schneider and Eggler, 1984; Mysen and Wheeler, 2000). Furthermore, water dissolved in silicate melts at high temperature and pressure often partially exsolved during quenching of melt to a glass at ambient temperature and

pressure. This exsolution can cause changes of water content and perhaps even D/H ratio of the quenched melt compared with its high-temperature/-pressure equilibrium values (Yoder et al., 1957; Hamilton et al., 1964; Eggler and Burnham, 1984; Mysen and Wheeler, 2000).

Many of the experimental and analytical complications attendant to determine isotope fractionation between melts and fluid from analysis of materials formed by quenching of high-temperature/-pressure experiments can be overcome by conducting the analyses while the samples are at the pressure and temperature of interest. This can be accomplished by containing the sample in an externally-heated diamond anvil cell (Bassett et al., 1996) with vibrational spectroscopy as the tool for isotopic analysis (Foustoukos and Mysen, 2012). For D/H fractionation, vibrational spectroscopy is particularly powerful because the frequency separation of vibrations involving D- and H-containing functional groups in melts and fluids can differ by as much as ~40% thus providing good peak separation without interference of neighboring peaks. This is the case, for example, for OH and OD vibrations (e.g., Walrafen, 1968; Walrafen et al., 1996). The objective of the present report is, therefore, to report experimentally-determined D/H fractionation between coexisting melt and fluid, *in-situ*, in isotopic equilibrium, and measured spectroscopically while the fluid and melt were at desired temperatures and pressures in an externally-heated diamond anvil cell.

Experimental Methods

Starting Compositions

Given the H_2O-rich nature of andesitic volcanism in subduction zone settings (e.g., Kushiro, 1972, 1990; Tatsumi, 1986; Grove et al., 2002), a study of the D/H fractionation between melts and aqueous fluids in hydrous silicate systems is appropriate. Haploandesitic compositions in the system Na_2O-Al_2O_3-SiO_2 with an Na/(Si+Al)-ratio that defines the degree of polymerization of dry melt (expressed as NBO/T) near that typical of andesitic melts (NBO/T=0.5) were, therefore, chosen. One composition, NS4, was Al-free and the other contained 10 mol % Al_2O_3 (NA10). These compositions were chosen in order to evaluate whether Al^{3+} may affect the D/H fractionation behavior. Furthermore, the liquidus and glass transition temperatures are for these two compositions are sufficiently low so that under the water-saturated conditions, the NS4 and NA10 materials are liquid over temperature ranges exceeding 500˚C within the temperature range attainable (≤1000˚C; Bassett et al., 1996) with the hydrothermal diamond anvil cell (Richet and Bottinga, 1984; Knoche et al., 1994; Del Gaudio et al., 2007). These two starting compositions were glasses from the starting materials originally used by Mysen (2007).

It must be remembered that these simple model systems and are aimed at elucidating principles. However, the principles derived from the simple system approach are directly applicable to characterization of isotope fraction in natural hydrous magmatic systems. Quantitative application to hydrous magmatic systems should, therefore, be carried out with caution.

Spectroscopic methods

The samples of coexisting melt and fluid, while at desired temperature and pressure, were examined with a JASCO™ model NRS-3100 confocal microRaman spectrometer with a ~ 1μm diameter 532 nm laser operating at ~ 7 mW at the sample for Raman excitation. Spectra are recorded through a 50X magnification/0.42 N.A. long-working distance Mitutoyo™ objective lens. An Andor™ Model DV401-F1 1024x128 pixel (25 μm pixel size) Peltier-cooled CCD was used for signal detection. The NRS-3100 Raman spectrometer is equipped with a single monochromator, a holographic notch filter, and holographic gratings with 600, 1200, and 2400 gratings/mm available for use. For the sample measurements (melt and fluid), 600 gratings/mm were used, which gives a CCD energy window corresponding to ~ 3650 cm^{-1}. The window center was positioned to record the spectra in one window from 200 to 3850 cm^{-1}. This spectral range is sufficient to encompass the entire frequency range of interest within a single CCD window (silicate, deuterated and protonated bond environments). The frequency resolution with this setting is 3-4 cm^{-1}. To measure the Raman spectra of ^{13}C diamond for pressure estimates, 2400 gratings/mm were employed and using Ne emission lines for internal frequency calibration.

High-pressure/-temperature experimental method

An externally-heated (Mo furnace winding) diamond anvil cell (HDAC) of the design originally described by Bassett et al. (1994, 1996) was employed. Iridium gaskets (125 μm thick and 500μm diameter sample-containing gasket hole) were used for sample containment. Temperatures were monitored and controlled to within ±1˚C with chromel-

alumel thermocouples. Pressure, generated by the fluid in the Ir gasket sample hole, was monitored in two different ways. In one, it was assumed that the equation-of-state of the silicate-saturated aqueous fluid can be approximated with that of pure H_2O (using PVT data from Wagner and Pruss, 2002). In the other method, pressure was derived by monitoring the temperature-/pressure-dependent one-phonon Raman shift of synthetic ^{13}C diamond (Schiferl et al., 1997; Mysen and Yamashita, 2010). These two methods were applied in a manner identical to that described by Mysen (2010a) except that when used to estimate pressure in the present study, it is also assumed that silicate-saturated, mixed H_2O+D_2O fluid has the same PVT properties as pure H_2O. Additional information of how these two methods are used to monitor pressure is described elsewhere (Bassett et al., 1996; Schiferl et al., 1997; Mysen and Yamashita, 2010). This information is not repeated here except to note that with the ^{13}C diamond pressure sensor the uncertainty governed by the accuracy of the Raman spectrometer calibrated with Ne emission lines recorded together with the Raman spectrum of the diamond is ±40 MPa (Mysen and Yamashita, 2010).

Silicate glass chips, ^{13}C diamond chips, and a 70 μm diameter by ~200 μm long rod of Pt metal (to enhance equilibration rate; Horita, 1988; – see also below) were loaded together with a 50:50 mixture (by volume) of H_2O+D_2O in the Ir gasket hole of the diamond anvil cell before high temperature/pressure experiments (Fig. 1). The D_2O+H_2O fluid mixture was made by stirring an approximately 5 ml mixture for about 1 hour before use. Fluid from the same batch of H_2O+D_2O fluid mixture was used in all experiments.

The experiments were conducted by first bringing the sample to the supercritical temperature and pressure region followed by a temperature and pressure decrease to conditions where melt and fluid coexist. In the present study, 800˚C was sufficient to reach supercritical conditions and 750˚C the highest temperature where melt and fluid coexist. The 750˚C temperature was, therefore, the highest temperature (and associated pressure) that could be studied in the present experiments. Following Raman spectroscopy of supercritical fluid, the temperature was decreased 750˚C for the highest temperature and pressure analysis of coexisting fluid and melt and then brought to successively lower temperature in 100˚C temperature decrements (cooling at 1˚C/s) (and lowering of the pressure as governed by the fixed sample volume in these experiments). The spectroscopic measurements were made at each temperature and pressure before these were lowered further. Time studies were also carried out at each temperature and pressure before changing the experimental conditions. The same sample was, therefore, used for all temperatures and pressures.

The temperature-dependent pressure trajectories of the experimental P/T sequences used in the present study (with NS4 and NA10 compositions, respectively) are shown in Fig. 2 with the pressures calculated assuming fluid PVT properties to be the same as those of pure H_2O (H_2O data from Wagner and Pruss, 2002) and from the one-phonon Raman shift of the ^{13}C synthetic diamond (Fig. 2). The P/T trajectories of the two series of experiments differ significantly because of their significantly different calculated fluid density (Table 1). The lower density for the NS4 experiments was necessary to attain similar temperature ranges of coexisting melt and fluid for both compositions.

The difference between the PVT-based and ^{13}C diamond-based trajectories is because silicate dissolved in the aqueous fluid coexisting with melt (Manning, 1994; Newton and Manning, 2008) and this silicate solute affects the fluid PVT properties (Mysen, 2010b). Different PVT properties of H_2O+D_2O fluid as compared with pure H_2O (Bazaev et al., 2003) might also contribute to the differences.

D/H ratio of coexisting melt and fluid

The ratio of integrated Raman intensities in the frequency range of OD and OH stretching (2400-2800 and 3400-3800 cm^{-1}, respectively) in the temperature and pressure range of the present experiments was used as a measure of the D/H ratio of a melt and fluid so that (Fig. 3),

$$(D/H)=A_{OD\ stretching}/A_{OH\ stretching}. \quad (1)$$

The principle behind eqn. (1) is the same as that used to determine D/H ratios in natural water samples (Lis et al., 2008).

Eqn. (1) relies on the assumption that the force constants for OD and OH stretching are the same so that these force constants cancel out and the ratio of integrated areas equals the abundance ratio of deuterated and pronated species. This assumption was tested with the Raman spectra of supercritical fluid with, therefore, only this silicate+fluid containing phase present in the diamond cell. The D_2O/H_2O volume ratio of the fluid added to the experimental charges equals 1, which translates to a molar D_2O/H_2O =0.9. The ratio of integrated areas (Fig. 3) from a spectrum of supercritical

NA10 fluid recorded at 800˚C and 1567 MPa (Fig. 3), $A_{OD\ stretching}/A_{OH\ stretching}$ = 0.87±0.05. This value is within error equal to the molar ratio of the D_2O+H_2O fluid. Equation (1) is, therefore, validated.

The frequency range of Raman bands assigned to OD stretching partly is within the frequency range of 2nd order Raman bands of diamond from the diamond cell itself. Their intensity was measured at the same temperature and pressure as the sample and then subtracted from the spectra of melt and fluid. The integrated areas, $A_{OD\ stretching}$ and $A_{OH\ stretching}$, were determined by summing up fitted bands of Voigtian line shape. The errors in these areas are the result of progression of fitting errors.

Equilibrium considerations

In order to promote isotopic equilibrium between melt and fluid, small rods of Pt metal were added to each of the samples because Pt greatly enhances the rate of isotope exchange (Horita, 1988). For example, it has been shown that D/H equilibrium between liquid H_2O and H_2 at 25˚C and ambient pressure is reached within 1-2 hrs (Horita, 1988). The current experiments were conducted with durations from about an hour to as much as 11 hours at each temperature and pressure (Table 1). In addition, to ensure that equilibrium was reached, time studies were carried out. Results from time study experiments at the lowest temperature and pressure of the experimental protocol (450˚C/101 MPa) indicate that constant D/H fractionation between coexisting melt and fluid was reached within minutes (Fig. 4). At higher temperatures, where diffusion rates are faster, even less time would be needed to reach equilibrium. We conclude, therefore,

that the experimental data reported here, and are from experiments of 1 hour or more, reflect isotopic equilibrium.

Hydrogen and deuterium mobility

Notably the D/H ratio of the D_2O+H_2O starting fluid and of the supercritical silicate (0.87±0.03 - recorded within about 30 minutes of reaching the actual temperature and pressure) is greater than that of fluid and melt recorded later in the experimental sequence (as much as several hours later). Mass balance considerations require, therefore, that either there is a third phase with D/H>0.87 or some H+D is lost from the system. The sink could be Pt or Ir, diamond in the diamond cell and in the ^{13}C polycrystalline diamond chips used for pressure measurements, or it could be in the quartz at least in the NS4 experiments. The quartz in the NS4 experiments is unlikely because of its low abundance (see above), is not observed in the NA10 experiments, and does not have detectable hydrogen or deuterium. However, hydrogen and deuterium could be dissolved in any and all the other phases (Pt, Ir, and diamonds). Which phases and how much cannot be ascertained given the sub-μg mass of the total sample in the diamond cell and, therefore, much smaller proportions of potentially dissolved hydrogen and deuterium in the other phases. Whichever hydrogen+deuterium loss-process is the cause of the lowered D/H ratio, this process is quite fast because time studies (Fig. 4) indicate that constant values are reached within a few tens of minutes.

Results

Experiments were conducted from 450˚ to 800˚C. At 800˚C, a single supercritical fluid existed. A few degrees above 750˚C is the highest temperature (and pressure) where fluid and melt coexist so D/H fractionation between fluid and melt was determined between 750˚ and 450˚C and corresponding pressures (Table 1). The considerably lower fluid density of the NS4 experiments (H_2O equivalent density=0.697 g/cm^3) than for NA10 (H_2O equivalent density=0.862 g/cm^3) was necessary to create a temperature range of coexisting melt and fluid comparable to that of the experiments with the NA10 system.

Several percent quartz was present in experiments with the NS4 composition across the entire temperature and pressure interval studied, similar to observations made by Mysen (2009) in an *in-situ* study of melt and fluid in the system NS4-H_2O. For the NA10 composition, quartz was not observed.

The presence of quartz necessarily results in an Na/Si increase of the melt + fluid portion of the system. Modal proportions of quartz (and melt and fluid) cannot be determined with precision in the hydrothermal diamond anvil cell, but a visual estimate is that the proportion of quartz is <5 volume % (with perhaps as much as a 50 % uncertainty). Growth of quartz with decreasing temperature can be observed optically so this proportion is the highest at the lowest temperature. By using 5 volume % as a maximum modal abundance, this translates to ~ 3.5 mol %. Consequently, the SiO_2 content of the NS4 + H_2O + D_2O system during the high temperature/pressure experiments could be as low as ~76.5±1.25 mol% by assuming a 50% uncertainty in the volume estimate of quartz.

In the Raman spectra, there are two frequency regions of interest. In the high-frequency region, between about 2400 and 3800 cm^{-1}, the dominant Raman bands are those assigned to OD and OH stretch vibration (Figs. 5, 6). These vibrations can be from molecular D_2O and H_2O and from OD and OH groups that form bonds with components of the silicate structure (e.g., Na^+, Al^{3+}, and Si^{4+}). In the low-frequency region, between about 200 and 1200 cm^{-1}, the principal Raman intensity is assigned to (Si,Al)-O vibrations. The Raman spectra in this frequency regime provide information on silicate structure in the (D_2O+H_2O)-saturated melts and of silicate in coexisting silicate-saturated (D_2O+H_2O) fluid (Figs. 7, 8).

The spectral data from the high-frequency region will be presented first because this is where information relevant to D/H fractionation between melts and fluids, which is the principal focus of this study, may be extracted. Raman data from the low-frequency region will then be presented as these data provide information necessary to characterize the D/H fractionation behavior.

High-frequency region

A few examples of Raman spectra of coexisting melt and fluid are shown in Fig. 5 with experimental temperature and pressure conditions indicated on the individual spectra. The group of Raman bands due to vibrations in OD and OH groups are marked "OD" and "OH". Also shown is a spectrum of H_2O+D_2O fluid with 2.4 molal H_2 recorded at conditions comparable to those of the present experiments (Foustoukos and Mysen, 2012). The peaks marked D_2 and HD in the latter spectrum are not of interest here and should be

277 ignored (the H_2 peak is near 4150 cm^{-1}, and is not, therefore shown in the spectra in Fig.
278 5).

279 The OD region (2400-2800 cm^{-1}) in spectra of melts and fluids characteristically
280 comprises 3-4 individual bands. This spectral region differs from the spectrum of
281 D_2O+H_2O fluid without silicate solute, which has only two peaks in this frequency region
282 (Fig. 5).

283 The Raman bands occur at the same frequency in spectra of both melt and fluid.
284 There is, however, distinctly less intensity in the lower-frequency portion of the envelope
285 in the spectra of melts. In the frequency range assigned to OH stretch vibrations (~3400-
286 3800 cm^{-1}), there is less spectral resolution and less difference between the spectra of
287 melts and coexisting fluids than in the frequency region of OD stretching. Furthermore,
288 asymmetry of these envelope to lower frequency, which is common in spectra of liquid
289 D_2O and D_2O+H_2O and H_2O at several hundred degrees lower temperature (Walrafen,
290 1968; Frantz et al., 1993; Walrafen et al., 1996; Kawamoto et al., 2004; Mysen, 2010a, b),
291 is absent at the temperatures of the present experiments (450˚C and higher).

292 The Raman intensity envelope between ~2400 and 3800 cm^{-1} can be deconvoluted to
293 add additional assignment details (Fig. 6). In analogy with the spectrum of high-
294 temperature/-pressure D_2O+H_2O, H_2O, and D_2O samples, the band near 3580 cm^{-1} is
295 assigned to OH vibrations in molecular H_2O and that near 3620 cm^{-1} to OH vibrations in
296 HDO (Walrafen, 1968, 1971; Ratcliffe and Irish, 1982; Kohl et al., 1991; Foustoukos and
297 Mysen, 2012) with the corresponding OD vibrations (from D_2O and HDO) likely are
298 those near 2600 and 2620 cm^{-1}, respectively (Walrafen, 1971; Max and Chapados, 2002;
299 Foustoukos and Mysen, 2012). The remaining bands in the OH envelope, near 3520 and

300 3640 cm^{1}, likely should be assigned to OH vibrations in OH groups associated with Na^{+}
301 (near 3520 cm^{-1}) and Si^{4+} (near 3640 cm^{-1}) (Mysen and Virgo, 1986; Cody et al., 2005).
302 By analogy (little independent experimental data are available), the 2550 and 2650 cm^{-1}
303 bands in the OD envelope probably should be assigned OD vibrations in complexes
304 associated with Na^{+} and Si^{4+}, respectively.
305
306 *Low-frequency region*
307 The low-frequency region (~200-~1200 cm^{-1}) comprises three frequency ranges of broad
308 Raman intensity, between 400 and 600 cm^{-1}, between 700 and 900 cm^{-1} and between
309 about 1000 and 1200 cm^{-1} (Fig. 7). Between 400 and 600 cm^{-1} the intensity envelope
310 consists of two or more individual bands. This envelope is more intense in the spectra of
311 hydrous melts than in spectra of silicate-saturated fluids. Strong Raman intensity in this
312 frequency region is common in spectra of glasses and melts of alkali and alkali
313 aluminosilicates (e.g., McMillan et al., 1992; Mysen et al., 2003; Neuville, 2006; Malfait
314 et al., 2007). In the mid-frequency range, between 700 and 900 cm^{-1}, there is also
315 intensity in spectra of melts and fluids. In spectra of fluid, the dominant peak is near 770
316 cm^{-1}, which is similar to Raman spectra of from other silicate-rich aqueous fluids under
317 similar pressure and temperature conditions (Zotov and Keppler, 2000, 2002; Mibe et al.,
318 2008; Mysen, 2009, 2010a, b). This peak is also seen in most of the spectra of hydrous
319 melts, but is much less intense than in spectra of fluid. In fact, in the melt spectra, the
320 dominant intensity in the 700-900 cm^{-1} region is between about 800 and 900 cm^{-1}. The
321 broad Raman intensity envelope between 1000 and 1200 cm^{-1} is dominant in the spectra
322 of NS4 hydrous melts, and much less so in NS4 silicate-saturated fluids and in NA10

fluids and melts (Fig. 7). Strong Raman bands in this region are characteristic of Raman spectra of alkali and alkaline earth silicate and aluminosilicate glasses and melts whether anhydrous or hydrous (e.g., Etchepare, 1972; McMillan, 1984; Frantz and Mysen, 1995; Mysen, 2007).

The structure of alkali silicate and alkali aluminosilicate glasses and melts has been discussed extensively (see, for example, Mysen and Richet, 2005, chs. 7 and 9, for a recent review of this literature). The Raman intensity in the 400-600 cm^{-1} frequency region commonly is assigned to Si-O-Si bending and rocking vibrations. The frequency decreases with increasingly polymerized structural units in a melt (Furukawa et al., 1981; Kubicki et al., 1992; McMillan and Wolf, 1995). The intensity in this spectral region indicates, therefore, the presence of polymerized silicate units. In the spectra of fluid this intensity diminishes as the temperature and pressure decrease. It is absent at the lowest temperatures and pressures of the present experiments (450˚C/101 MPa) (Fig. 7). This spectral evolution is qualitatively similar to that observed in Raman spectra of fluids from other hydrous silicate systems (Zotov and Keppler, 2000, 2002; Mibe et al., 2008).

The Raman bands in the frequency region above 700 cm^{-1} have been fitted to Voigt curves with two examples shown in Fig. 8 (for coexisting melt and fluid). The band near 770 cm^{-1} is assigned to Si-O^- (O^-; nonbridging oxygen) in Q^0 species. Those near 820 and 880 cm^{-1} are assigned to similar vibrations in more polymerized Q-species (Q^1 and Q^2, respectively, e.g., Zotov and Keppler, 2002; Yamashita et al., 2007; Mibe et al., 2008; Mysen, 2009, 2010a). The Raman band near 980 cm^{-1} is assigned to Si-OH stretching (e.g., Stolen and Walrafen, 1976; McMillan and Remmele, 1986). Finally, the band near 1050 cm^{-1}, observed in Raman spectra of all melts and glasses that contain bridging

This is a preprint, the final version is subject to change, of the American Mineralogist (MSA)
Cite as Authors (Year) Title. American Mineralogist, in press.
(DOI will not work until issue is live.) DOI: http://dx.doi.org/10.2138/am.2013.4247

oxygen likely is an Si-O^0 vibration (e.g., (e.g., Bell et al., 1970; Brawer and White, 1975, 1977; Furukawa et al., 1981; Mysen et al., 1982; Fukumi et al., 1990; McMillan et al., 1992).

Discussion

The D/H abundance ratio of coexisting fluids and melts as a function of temperature, pressure, and composition were extracted from the Raman spectra by using eqn. (1) as discussed above (Fig. 9). The D/H ratio with temperature from these measurements and was fitted to an expression of the form,

$$\ln(D/H)=a+b/T, \quad (2)$$

where T is temperature (K) and D/H is the mol fraction ratio of deuterated and protonated OD and OH groups, respectively. In fluids, this ratio is positively correlated with temperature, whereas for coexisting melts, there is no clear relationship between D/H ratio and temperature (Fig. 9).

The regression parameters and derived enthalpy of the D H exchange are given in Table 2. Notably, for fluid the ΔH derived from the slope in Fig. 9 differs significantly from 0 (3.1±0.8 and 5.2±0.9 kJ/mol for NS4 and NA10 compositions, respectively), whereas for melt in both compositions ΔH is indistinguishable from 0 (NA10) or has a very small value with a large error (NS4: ΔH=-1.5±0.8 kJ/mol).

For the D/H exchange equilibrium between fluid and melt;

369

370 $$H_2O(melt)+D_2O(fluid) \rightleftharpoons H_2O(fluid)+D_2O(melt), \quad (3)$$

371

372 the exchange equilibrium constant is,

373

374 $$K^{D/H}(melt-fluid)=\frac{[D_2O(melt)][H_2O(fluid)]}{[D_2O(fluid)][H_2O(melt)]}=\frac{\left[\frac{D}{H}\right](melt)}{\left[\frac{D}{H}\right](fluid)}. \quad (4)$$

375

376 The D/H-ratios in eqn (4) are equivalent to D_2O/H_2O and the D/H ratios in in Fig. 9 yield
377 the results in Fig. 10.

378 The exchange equilibrium constant, $K^{D/H}$(melt-fluid), can then be fitted to an
379 expression similar to eqn. (2) to yield the enthalpy change of reaction (3);

380

381 $$\ln K^{D/H} = a+b/T, \quad (5)$$

382

383 with regression coefficients in Table 2.

384 The results in Figs. 9 and 10 reflect both temperature and pressure-dependence of the
385 D–H equilibria in and between fluids and melts together with possible effects on the
386 melt and fluid composition of temperature and pressure. The possible pressure effect
387 exists because in these experiments, pressure is a variable that is a positive function of
388 temperature (Fig. 2). In addition, the solubility and structure of silicate in the fluid and
389 D_2O+H_2O in melt depend on pressure and temperature (e.g., Hamilton et al., 1964;
390 Nowak and Behrens, 1995; Newton and Manning, 2002, 2007; Mysen, 2010b; Holtz et

al., 2000). For melts, the main temperature (and pressure) effect is an increase in total H_2O+D_2O concentration.

By assuming that D_2O and H_2O have similar effects on the structure of silicate melts and also form similar species in the melt, I will refer to this total D_2O+H_2O as water and discuss its behavior as if it simply is H_2O. Water dissolved in silicate melts exists both in molecular form and as OH groups that form bonds with components of the silicate network. In the present melts, Na-OH, Na-OD, Si-OH and Si-OD bonds likely exist. Only these OH-groups (and OD) affects the silicate structure and, therefore, properties of hydrous silicate melts. Here, I will simply refer to this as OH (structural details of the different effects of Na-OH and Si-OH bonding in melts can be found in Cody et al., 2005).

A significant fraction of dissolved water (and deuterated water – see discussion above) is in molecular form, which is referred to simply as H_2O in this discussion. The OH/H_2O ratio varies with total water content and to some extent with melt composition (e.g., Stolper, 1982; Dixon et al., 1991; Hui et al., 2009). Its rate of increase decreases rapidly with increasing total water content at any temperature, pressure, and melt composition (e.g., Dixon et al., 1991; Hui et al., 2009). The OH abundance approaches a maximum between 3 and 4 wt %, calculated as H_2O, which is reached with total water content near 4-5 wt% (Nowak and Behrens, 1995, 2001). Any further increase in total water content results in only minor changes in OH concentration. Most additional water dissolved in silicate melts exists in molecular form.

Even at the lowest temperature and pressure of the present experiments (450˚C and 101 MPa for NS4 composition), the total H_2O concentration is 4-5 wt% (Calculated with

414 the empirical algorithm of Moore et al., 1998). This means that for all practical purposes,
415 the total OH concentration in melts in all of the experiments discussed in this report, and
416 which were at higher temperature and pressure, does not vary significantly. This
417 conclusion, in turn, implies that the effect of dissolved water on melt properties that
418 depend on melt structure would be nearly the same once the total water content reaches
419 4-5 wt%. An example of a melt property evolution with water content is the degree of
420 silicate polymerization, which can be quantified with the parameter, NBO/T (nonbridging
421 oxygen per tetrahedrally coordinated cation – here Al^{3+} and Si^{4+}). The NBO/T is nearly
422 constant (Fig. 11). Consequently, if D/H fractionation of hydrous silicate melts depends
423 on the silicate melt structure, one would expect little effect of water at concentrations
424 concentration higher than about 5 wt%. This is exactly what was observed (Fig. 9).

425 The relationship between polymerization of silicate solute in aqueous solution and
426 temperature and pressure results in NBO/T-variations that differ from silicate
427 polymerization characteristics of hydrous melts. In silicate-rich aqueous fluid this silicate
428 becomes increasingly polymerized (decreasing NBO/T) with increasing temperature and
429 pressure in contrast to the NBO/T-behavior of silicate melt (Fig. 11). This behavior is
430 because the total silicate content in the fluid increases with temperature and pressure and
431 in analogy anhydrous silicate melt becomes increasingly polymerized with increasing
432 total silicate concentration (e.g., Maekawa et al., 1991). Although the bulk silicate
433 content of the aqueous fluid is not known, the evolution of the Q-species and NBO/T of
434 the silicate is (Table 3). It is proposed that it is this change in silicate solute concentration
435 and structure that causes the (D/H)(fluid) to be more sensitive to temperature and
436 pressure than the D/H-ratio in coexisting melt. This effect, in turn, underlies the

temperature effect of the $K^{D/H}$(melt-fluid) (Fig. 10). This behavior is also analogous to oxygen fractionation between CO_2 and aqueous fluids with various salts in solution where type and concentration of salt solutes has major effects on oxygen isotope fractionation between solution and CO_2 (O'Neil and Truesdell, 1991; O'Neil et al., 2003). □□□□□□□□□□□□□□□□□□□□□□□□□□□□□□□□□□□□□□D/H fractionation between fluid and condensed phases (melts and minerals) at temperature and pressure conditions of high-grade metamorphism and of hydrous partial melting in the Earth's upper mantle (e.g., above subduction zones), the silicate solute concentration and structure in the fluid can have major effects on the fractionation factors.

Acknowledgements

This research was partially supported by NSF grants EAR-0734182 and EAR-1212754 and a NASA astrobiology Institute. A grant from the W. M. Keck Foundation supported acquisition of the Jasco IRS-3100 microRaman spectrometer. The ^{13}C diamond was synthesized by Li Zhang. Her assistance is greatly appreciated.

References

Bassett, W.A., Shen, A.H., Bucknum, M., Chou, I.M., 1994. A new diamond cell for hydrothermal studies to 2.5 GPa from -190˚C to 1200˚C. Reviews of Scientific Instruments 64, 2340-2345.

Bassett, W.A., Wu, T.-C., Chou, I.-M., Haselton, T., Frantz, J.D., Mysen, B.O., Huang, W.-L., Sharma, S.K., Schiferl, D., 1996. The hydrothermal diamond anvil cell (DAC) and its applications, in: Dyar, M.D., McCammon, C.A., Schaefer, M. (Eds.), Mineral Spectroscopy: A Tribute to Roger G. Burns. The Geochemical Society, Houston, pp. 261-272.

Bazaev, A. R., Abdulagatov, I. M., Magee, J. W., Bazaev, E. A. and Ramazanova, A. E., 2003. PVTx measurements for H_2O+D_2O mixtures in the near-critical and supercritical regions, Journal of Supercritical Fluids 26, 115-128.

Bell, R. J., Dean, D. P. and Hibbins-Butler, D. C., 1970. Localization of normal modes in vitreous silica, germania, and beryllium fluoride, Journal of Physical Chemistry 3, 2111-2118.

Brawer, S.A., White, W.B., 1975. Raman spectroscopic investigation of the structure of silicate glasses. I. the binary silicate glasses. Journal of Chemical Physics63, 2421-2432.

Brawer, S.A., White, W.B., 1977. Raman spectroscopic investigation of the structure of silicate glasses. II. The soda-alkaline earth-alumina ternary and quaternary glasses. Journal of Non-Crystalline Solids 23, 261-278.

Cody, G.D., Mysen, B.O., Lee, S.K., 2005. Structure vs. composition: A solid state ^{1}H and ^{29}Si NMR study of quenched glasses along the Na_2O-SiO_2-H_2O join. Geochimica et Cosmochimica Acta 69, 2373-2384.

Del Gaudio, P., Behrens, H., Duebner, J., 2007. Viscosity and glass transition temperature of hydrous float glass. Journal of Non-Crystalline Solids 353, 223-236.

Dixon, J.D., 1997. Degassing of alkalic basalts. Amer Mineral. 82, 368-378.

Dixon, J.E., Clague, D.A., Stolper, E.M., 1991. Degassing history of water, sulfur, and carbon in submarine lavas from Kilauea volcano, Hawaii. Journal of Geology 99, 371-394.

Dobson, P.F., Epstein, S., Stolper, E.M., 1989. Hydrogen isotope fractionation between coexisting vapor and silicate glasses and melts at low pressure. Geochimica et Cosmochimica Acta 53, 2723-2731.

Eggler, D.H., Burnham, C.W., 1984. Solution of H_2O in diopside melts: a thermodynamic model, Contributions to Mineralogy and Petrology 85, 58-66.

Etchepare, J., 1972. Study by Raman spectroscopy of crystalline and glassy diopside, in: Douglas, R.W., Ellis, E. (Eds.), Amorphous Materials. Wiley-Interscience, pp. 337-346.

Exley, R.A., Boyd, S.R., Mattey, D.P., Pillinger, C.T., 1987. Nitrogen isotope geochemistry of basaltic glasses: implications for mantle degassing and structure? Earth and Planetary Science Letters 81, 163-174.

Foustoukos, D.I., Mysen, B.O., 2012. D/H fractionation in the H_2-H_2O system at supercritical water conditions: Compositional and hydrogen bonding effects. Geochimica et Cosmochimica Acta 86, 88-102.

Frantz, J.D., Mysen, B.O., 1995. Raman spectra and structure of BaO-SiO_2, SrO-SiO_2, and CaO-SiO_2 melts to 1600˚C. Chemical Geology 121, 155-176.

Frantz, J.D., Dubessy, J., Mysen, B., 1993. An optical cell for Raman spectroscopic studies of supercritical fluids and its applications to the study of water to 500 °c and 2000 bar. Chemical Geology 106, 9-26.

Fukumi, K., Hayakawa, J., Komiyama, T., 1990. Intensity of Raman band in silicate glasses. Journal of Non-Crystalline Solids 119, 297-302.

Furukawa, T., Fox, K.E., White, W.B., 1981. Raman spectroscopic investigation of the structure of silicate glasses. III. Raman intensities and structural units in sodium silicate glasses. Journal of Chemical Physics153, 3226-3237.

Grove, T.L., Parman, S.W., Bowring , S.A., Price, R.C., Baker, M.B., 2002. The role of H_2O-rich fluid component in the generation of primitive basaltic andesites and andesites from the Mt. Shasta region, N California. Contributions to Mineralogy and Petrology 142, 375-396.

Hamilton, D.L., Burnham, C.W., Osborn, E.F., 1964. The solubility of water and the effects of oxygen fugacity and water content on crystallization of mafic magmas. Journal of Petrology 5, 21-39.

Hauri, E.H., 2002. SIMS analysis of volatiles in silicate glasses, 2: isotopes and abundances in Hawaiian melt inclusions. Chemical Geology 183, 115-141.

Holtz, F., Roux, J., Behrens, H., Pichavant, M., 2000. Water solubility in silica and quartzofeldspathic melts. American Mineralogist 85, 682-686.

Horita, J., 1988. Hydrogen isotope analyses of natural waters using an H_2-water equilibration method: A special implication to brines. Chemical Geology 72, 89-94.

Hui, H., Zhang, Y., Xu, Z., Del Gaudio, P., Behrens, H., 2009. Pressure dependence of viscosity of rhyolitic melts Geochimica et Cosmochimica Acta 73, 3680-3693.

Kasting, J.F., Eggler, D.H., Raeburn, S.P., 1993. Mantle redox evolution and the oxidation state of the Archean atmosphere. Journal of Geology 101, 245-257.

Kawamoto, T., Ochiai, S., Kagi, H., 2004. Changes in the structure of water deduced from the pressure dependence of the Raman OH frequency. Journal of Chemical Physics 120, 5867-5870.

Knoche, R., Dingwell, D.B., Seifert, F.A., Webb, S.L., 1994. Non-linear properties of supercooled liquids in the system Na_2O-SiO_2. Chemical Geology 116, 1-16.

Kohl, W., Lindner, H.A., Franck., E.U., 1991. Raman spectra of water to 400˚C and 3000 bar. Berichte Bundesenges Physique und Chemie. 95, 1586-1593.

Kubicki, J.D., Hemley, R.J., Hofmeister, A.M., 1992. Raman and infrared study of pressure-induced structural changes in $MgSiO_3$, $CaMgSi_2O_6$, and $CaSiO_3$ glasses. American Mineralogist 77, 258-269.

Kuroda, Y., Kariya, Y., Suzuoki, T., Matsuo, S., 1982. D/H fractionation between water and the melts of quartz, K-feldspar, albite and anorrthite at high temperature and pressure. Geochemical Journal 16, 73-78.

Kushiro, I., 1972. Effect of water on the composition of magmas formed at high pressures. Journal Petrol.ogy 13, 311-334.

Kushiro, I., 1990. Partial melting of mantle wedge and evolution of island arc crust. Journal of Geophysical Research 95, 15929-15939.

Lis, G., Wassenaar, L.I., Hendry, M.J., 2008. High-Precision Laser Spectroscopy D/H and $^{18}O/^{16}O$ Measurements of Microliter Natural Water Samples. Analytical Chemistry 80, 287-293.

Maekawa, H., Maekawa, T., Kawamura, K., Yokokawa, T., 1991. The structural groups of alkali silicate glasses determined from ^{29}Si MAS-NMR. Journal of Non-Crystalline Solids 127, 53-64.

Malfait, W.J., Zakaznova-Herzog, V.P., Halter, W.E., 2007. Quantitative Raman spectroscopy: High-temperature speciation of potassium silicate melts. Journal of Non-Crystalline Solids 353, 4029-4042.

Manning, C.E., 1994. The solubility of quartz in H_2O in the lower crust and upper mantle.

545 Geochimica et Cosmochimica Acta 58, 4831-4840.
546 Manning, C.E., 2004. The chemistry of subduction-zone fluids. Earth Planet. Sci. Lett. 223, 1-16.
547 Max, J.J., Chapados, C., 2002. Isotope effects in liquid water by infrared spectroscopy. Journal
548 of Chemical Physics 116, 4626-4642.
549 McMillan, P., 1984. Structural studies of silicate glasses and melts-- applications and limitations
550 of Raman spectroscopy. American Mineralogist 69, 622-644.
551 McMillan, P.F., Remmele, R.L., 1986. Hydroxyl sites in SiO_2 glass: A note on infrared and
552 Raman spectra. American Mineralogist 71, 772-778.
553 McMillan, P.F., Wolf, G.H., 1995. Vibrational spectroscopy of silicate liquids, in: Stebbins, J.F.,
554 McMillan, P.F., Dingwell, D.B. (Eds.), Structure, Dynamics and Properties of Silicate Melts.
555 Mineralogical Society of Washington, Washington DC, pp. 247-315.
556 McMillan, P.F., Wolf, G.H., Poe, B.T., 1992. Vibrational spectroscopy of silicate liquids and
557 glasses. Chemical Geology 96, 351-366.
558 Mibe, K., Chou, I.M., Bassett, W.A., 2008. In situ Raman spectroscopic investigation of the
559 structure of subduction-zone fluids. Journal of Geophysical Research 113, 1-8.
560 Moore, G., Vennemann, T., Carmichael, I.S.E., 1998. An empirical model for the solubility of
561 H2O in magmas to 3 kilobars. American Mineralogist 83, 36-42.
562 Mysen, B.O., 2007. The solution behavior of H_2O in peralkaline aluminosilicate melts at high
563 pressure with implications for properties of hydrous melts. Geochimica et Cosmochimica
564 Acta 71, 1820-1834.
565 Mysen, B.O., 2009. Solution mechanisms of silicate in aqueous fluid and H_2O in coexisting
566 silicate melts determined in-situ at high pressure and high temperature. Geochimica et
567 Cosmochimica Acta 73, 5748-5763.
568 Mysen, B.O., 2010a. Structure of H_2O-saturated peralkaline aluminosilicate melt and coexisting
569 aluminosilicate-saturated aqueous fluid determined in-situ to 800˚C and ~800 MPa.
570 Geochimica et Cosmochimica Acta 74, 4123-4139.
571 Mysen, B.O., 2010b. Speciation and mixing behavior of silica-saturated aqueous fluid at high
572 temperature and pressure. American Mineralogist 95, 1807-1816.
573 Mysen, B.O., Virgo, D., 1986. Volatiles in silicate melts at high pressure and temperature. 1.
574 Interaction between OH groups and Si^{4+}, A;$^{3+}$, Ca^{2+}, Na^{+} and H^{+}. Chemical Geology 57,
575 303-331.
576 Mysen, B.O., Wheeler, K., 2000. Solubility behavior of water in haploandesitic melts at high
577 pressure and high temperature. American Mineralogist 85, 1128-1142.
578 Mysen, B.O., Richet, P., 2005. Silicate Glasses and Melts - Properties and Structure. Elsevier,
579 New York. 564 pp.
580 Mysen, B.O., Yamashita, S., 2010. Speciation of reduced C-O-H volatiles in coexisting fluids
581 and silicate melts determined in-situ to ~1.4 GPa and 800˚C. Geochim. Cosmochim.
582 Geochimica et Cosmochimica Acta 74, 4577-4588.
583 Mysen, B.O., Virgo, D., Seifert, F.A., 1982. The structure of silicate melts; implications for
584 chemical and physical properties of natural magma. Reviews of Geophysics and Space
585 Physics 20, 353-383.
586 Mysen, B.O., Lucier, A., Cody, G.D., 2003. The structural behavior of Al^{3+} in peralkaline melts
587 and glasses in the system Na_2O-Al_2O_3-SiO_2. American Mineralogist 88, 1668-1678.
588 Neuville, D.R., 2006. Viscosity, structure and mixing in (Ca,Na) silicate melts. Chemical
589 Geology 229, 28-41.
590 Newton, R.C., Manning, C.E., 2002. Solubility of enstatite+forsterite in H_2O in deep crust/upper

591 mantle conditions: 4 to 15 kbar and 700 to 900˚C. Geochimica et Cosmochimica Acta 66,
592 4165-4176.
593 Newton, R.C., Manning, C.E., 2007. Solubility of grossular, $Ca_3Al_2Si_3O_{12}$, in H_2O-NaCl
594 solutions at 800˚C and 10 kbar, and the stability of garnet in the system $CaSiO_3$-Al_2O_3-H_2O-
595 NaCl. Geochimica et Cosmochimica Acta 71, 5191-5202.
596 Newton, R.C., Manning, C.E., 2008. Thermodynamics of SiO_2-H_2O fluid near the upper critical
597 end point from quartz solubility measurements at 10 kbar. Earth and Planetary Science
598 Letters 274, 241-249.
599 Nowak, M., Behrens, H., 1995. The speciation of water in haplogranitic glasses and melts by in-
600 situ, near-infrared spectroscopy. Geochimica et Cosmochimica Acta 59, 3445-3450.
601 Nowak, M., Behrens, H., 2001. Water in rhyolitic magmas: Getting a grip on a slippery problem.
602 Earth and Planetary Science Letters 184, 515-522.
603 O'Neil, J.R., Truesdell, A.E., 1991. Oxygen isotope fractionation studies of solute water
604 interactions, in: Taylor, H.P., O'Neil, J.R., Kaplan, I.R. (Eds.), Stable Isotope Geochemistry:
605 A Tribute to Samuel Epstein. The Geochemical Society, Calgary, pp. 17-25.
606 O'Neil, J.R., Vennemann, T.W., MacKenzie, W.F., 2003. Effects of speciation on equilibrium
607 fractionations and rates of oxygen isotope exchange between (PO_4)aq and H_2O. Geochimica
608 et Cosmochimica Acta 67, 3135-3144.
609 Pineau, F., Shilobreeva, S., Kadik, A., Javoy, M., 1998. Water solubility and D/H fractionation
610 in the system basaltic andesite-H_2O at 1250˚C and between 0.5 and 3 kbars. Chemical
611 Geology 147, 173-184.
612 Ratcliffe, C.I., Irish, D.E., 1982. Vibrational studies of solutions at elevated temperatures and
613 pressures. 5. Raman studies of liquid water up to 300 °C. Journal of Physical Chemistry 86,
614 4897-4905.
615 Richet, P., Bottinga, Y., 1984. Glass transitions and thermodynamic properties of amorphous
616 SiO_2, $NaAlSi_nO_{2n+2}$ and $KAlSi_3O_8$. Geochimica et Cosmochimica Acta 48, 453-471.
617 Richet, P., Roux, J., Pineau, F., 1986. Hydrogen isotope fractionation in the system H_2O-liquid
618 $NaAlSi_3O_8$: New data and comments on D/H fractionation in hydrothermal experiments.
619 Earth and Planetary Science Letters 78, 115-120.
620 Schiferl, D., Nicol, M., Zaug, J.M., Sharma, S.K., Cooney, T.F., Wang, S.-Y., Anthony, T.R.,
621 Fleischer, J.F., 1997. The diamond $^{13}C/^{12}C$ isotope Raman pressure sensor system for high
622 temperature/pressure diamond-anvil cells with reactive samples. Journal of Applied Physics
623 82, 3256-3265.
624 Schneider, M.E., Eggler, D.H., 1984. Compositions of fluids in equilibrium with peridotite:
625 implications for alkaline magmatism-metasomatism, in: Kornprobst, J. (Ed.), Kimberlites. I.
626 Kimberlites and Related Rocks. Elsevier, pp. 383-394.
627 Stolen, R.H., Walrafen, G.E., 1976. Water and its relation to broken bond defects in fused silica.
628 Journal of Chemical Physics 64, 2623-2631.
629 Stolper, E., 1982. The speciation of water in silicate melts. Geochimica et Cosmochimica Acta
630 46, 2609-2620.
631 Tatsumi, Y., 1986. Origin of subduction zone magmas based on experimental petrology, in:
632 Perchuk, L., Kushiro, I. (Eds.), Physics and Chemistry of Magmas. Springer, Berlin, pp. 268-
633 301.
634 Tolstikhin, I. N., and Marty, B., 1998. The evolution of terrestrial volatiles: a view from helium,
635 argon and nitrogen isotope modeling, Chemical Geology 147, 27-52.
636 Wagner, W., Pruss, A., 2002. The IAPWS formulation 1995 for the thermodynamic properties of

ordinary water substance for general scientific use. J. Phys. Chem. Ref. Data 31, 387-535.
Walrafen, G.E., 1968. Raman Spectral Studies of HDO in H_2O. Journal of Chemical Physics 48, 244.
Walrafen, G.E., 1971. Raman spectra from HDO in H_2O to 7.2 kbar. Journal of Physical Chemistry 55, 5137-5139.
Walrafen, G.E., Yang, W.H., Chu, Y.C., Hokmabadi, M.S., 1996. Raman OD-stretching overtone spectra from liquid D_2O between 22 and 152 decrees C. Journal of Physical Chemistry 100, 1381-1391.
Yamashita, S., Kanzaki, M., Mysen, B.O., 2007. In situ observation of silicate speciation in liquids in the system $K_2Si_4O_9$-H_2O at high temperature and high pressure (abstr), JPGU Annual Meeting, Chiba City, Japan.
Yoder, H.S., Stewart, D.B., Smith, J.R., 1957. Ternary feldspars. Carnegie Instn. Washington Year Book 56, 206-214.
Zotov, N., Keppler, H., 2000. In-situ Raman spectra of dissolved silica species in aqueous fluid to 900˚C and 14 kbar. American Mineralogist 85, 600-603.
Zotov, N., Keppler, H., 2002. Silica speciation in aqueous fluids at high pressures and high temperatures. Chemical Geology 184, 71-82.

This is a preprint, the final version is subject to change, of the American Mineralogist (MSA)
Cite as Authors (Year) Title. American Mineralogist, in press.
(DOI will not work until issue is live.) DOI: http://dx.doi.org/10.2138/am.2013.4247

Table 1. Run data

Composition	Temp.,˚C	Press, MPa	Duration, min	Phases present
NS4	850	492	120	supercritical fluid
NS4	750	420	0	melt+fluid*+qtz
NS4	750	420	75	melt+fluid+qtz
NS4	750	420	150	melt+fluid+qtz
NS4	750	420	210	melt+fluid+qtz
NS4	650	405	5	melt+fluid+qtz
NS4	650	405	75	melt+fluid+qtz
NS4	650	405	155	melt+fluid+qtz
NS4	650	405	210	melt+fluid+qtz
NS4	550	262	0	melt+fluid+qtz
NS4	550	262	75	melt+fluid+qtz
NS4	550	262	230	melt+fluid+qtz
NS4	550	262	380	melt+fluid+qtz
NS4	450	101	0	melt+fluid+qtz
NS4	450	101	95	melt+fluid+qtz
NS4	450	101	145	melt+fluid+qtz
NS4	450	101	1090	melt+fluid+qtz
NA10	800	1567	0	supercritical fluid
NA10	750	1381	120	melt+fluid**
NA10	675	1163	30	melt+fluid
NA10	600	1019	120	melt+fluid
NA10	525	764	130	melt+fluid
NA10	450	471	110	melt+fluid

*: Density of fluid during NS4 experiments calculated as pure H_2O: 0.697 g/cm^3
**: Density of fluid during NA10 experiments calculated as pure H_2O: 0.862 g/cm^3

Table 2. Coefficients for eqns. (3) and (5) and derived enthalpy change, ΔH (kJ/mol)

	Eqn(2): ln(D/H)=a+b/T				Eqn(5): $\ln K^{D/H}$(melt-fluid)=a+b/T			
	a	b	r^2	ΔH	a	b	r^2	ΔH
NS4(melt)	-0.80±0.12	88±105	0.62	-1.5±0.8	-0.58±0.10	558±86	0.95	4.6±0.7
NS4(fluid)	0.23±0.11	-369±94	0.89	3.1±0.8				
NA10(melt)	-0.51±0.27	68±229	0.03	0.6±2.0	-1.09±0.10	782±87	0.96	6.5±0.7
NA10(fluid)	0.47±0.13	-627±112	0.96	5.2±0.9				

Table 3 – Silicate species abundance in melt and coexisting fluid

Composition	Temp.,˚C	Press., MPa	Q^0	Q^1	Q^2	Q^3	NBO/T
			Melt				
NS4	750	420	0.13±0.06	0.23±0.04	0.63±0.09		2.5±0.2
NS4	650	405	0.04±0.02	0.45±0.17	0.50±0.2		2.5±0.4
NS4	550	262	0.04±0.01	0.65±0.1	0.07±0.02	0.24±0.2	2.5±0.2
NS4	450	101	0.03±0.01	0.44±0.18	0.31±0.11	0.22±0.11	2.3±0.3
NA10	750	1381	0.43±0.05	0.33±0.05	0.25±0.06		3.2±0.1
NA10	675	1163	0.35±0.09	0.35±0.03	0.30±0.03		3.1±0.1
NA10	600	1019	0.37±0.03	0.41±0.03	0.21±0.02		3.16±0.07
NA10	525	764	0.38±0.07	0.31±0.07	0.31±0.04		3.1±0.2
NA10	450	450	0.36±0.12	0.15±0.11	0.49±0.09		2.9±0.3
			Fluid				
NS4	750	420	0.7±0.3	0.06±0.02	0.24±0.06		3.5±0.4
NS4	650	405	0.68±0.04	0.16±0.02	0.16±0.04		3.51±0.08
NS4	550	262	0.8±0.2	0.15±0.03	0.04±0.01		3.8±0.3
NS4	450	101	1.00±0.08				4.00±0.08
NA10	750	1381	0.35±0.14	0.34±0.05	0.31±0.05		3.0±0.2
NA10	675	1163	0.49±0.13	0.29±0.12	0.22±0.11		3.3±0.3
NA10	600	1019	0.62±0.23	0.18±0.07	0.20±0.08		3.4±0.4
NA10	525	764	0.67±0.16	0.15±0.04	0.17±0.05		3.5±0.2
NA10	450	450	0.76±0.21	0.09±0.03	0.15±0.05		3.6±0.2

Figure Captions

Figure 1 – Microphotograph of NA10 + ^{13}Cdiamond + Pt rod + (H_2O+D_2O) sample loaded in the diamond cell before high-temperature/-pressure experiments

Figure 2 – Pressure-temperature trajectories of the NS4 (circles) and NA10 (squares) samples. Open symbols: Pressure calculated from temperature and assuming the same PVT properties as pure H_2O. Closed symbols: Pressure calculated from the one-phonon Raman shift of ^{13}C diamond. The pressure from the ^{13}C diamond is used throughout the text.

Figure 3 – Example of Raman spectrum showing Raman scattering from OD and OH vibrations ($A_{OD\ stretching}$ and $A_{OH\ stretching}$, respectively). The spectrum is from composition NA10 and was recorded with the sample at 800˚C and 1567 MPa where supercritical fluid, Pt rod and ^{13}C diamond coexist.

Figure 4 - Results of time study that shows the D/H fractionation between coexisting hydrous silicate melt and silicate-saturated aqueous fluid [$K^{D/H}$(melt-fluid)] as a function of experimental run duration (time) from experiments conducted at 450˚C and 101 MPa with NS4 composition.

Figure 5 – Examples of Raman spectra of coexisting hydrous silicate melt and silicate-saturated aqueous fluid in the frequency region that encompasses OD and OH stretching (marked "OD" and "OH", whether from structurally bound OD and OH or from molecular D_2O and H_2O). Conditions and composition of starting materials are indicated on individual figures. Coexisting melt and fluid are indicated with the same temperature and pressure on their spectra. Also shown is an example of a Raman spectrum in the same frequency range from the system H_2O-D_2O-H_2-D_2 (Foustoukos and Mysen, 2012) to illustrate the forms of the OD and OH signals from silicate-free fluid. See also text for further discussion.

Figure 6 - Example of curve-fitted Raman spectra of coexisting hydrous silicate melt and silicate-saturated aqueous fluid in the frequency region that encompasses OD and OH stretching from an experiment with composition NS4 at 750˚C and 420 MPa. See text for detailed description and discussion.

Figure 7 – Examples of curve-fitted Raman spectra of coexisting hydrous silicate melt and silicate-saturated aqueous fluid in the frequency region that encompasses Si(Al)-O vibrations. Conditions and composition of starting materials are indicated on individual figures. Coexisting melt and fluid are indicated by the same temperature and pressure.

Figure 8 - Example of curve-fitted Raman spectra of coexisting hydrous silicate melt and silicate-saturated aqueous fluid in the frequency region that encompasses Si(Al)-O vibrations from an experiment with composition NA10 at 675˚C and 1163 MPa. See text for detailed description and discussion.

Figure 9 - The D/H ratio [ratio of integrated areas of OD and OH stretching – see also eqn. (1)] of hydrous silicate melt and silicate-saturated aqueous fluid as a function of temperature for compositions NS4 and NA10 as indicated. Also shown is a data point for supercritical fluid of NA10 composition (see also Fig. 3 for Raman spectrum of this sample). Regression coefficients for eqn. (2) are given in Table 2 with their implications discussed in the text.

Figure 10 – Exchange equilibrium coefficient, $K^{D/H}$(melt-fluid) for equilibrium (3) as shown in eqn. (4) as a function of temperature. The regression coefficients for eqn. (5) are shown in Table 2 with the derived enthalpy change for equilibrium (3) shown on the individual graphs.

Figure 11 - Evolution of degree of silicate polymerization of silicate solvent in hydrous silicate melt (NS4(melt) and NA10(melt) and silicate solute in coexisting aqueous fluid (NS4(fluid) and NA10(fluid) as a function of temperature and pressure. Note that the pressure scale differs for the two compositions as discussed in the text. The NBO/T evolution was calculated from the Q-species abundance as discussed in the text.
The NBO/T of the melt and the silicate solute in the D_2O+H_2O fluids was derived from the Raman spectra using the methods described by Mysen (2010a), which, in turns, relied on calibration of relevant Raman intensities against ^{29}Si MAS NMR data by Cody et al. (2005). With this method, the proportion of individual Q-species were derived first (Table 3). These data are then employed to compute the NBO/T-values;

$$NBO/T = \sum_{n=0}^{n=4} X_{Q^n} \bullet (nbo/t)_{Q^n},$$

where X_{Q^n} and $(nbo/t)_{Q^n}$ are mol fraction of Q-species and the nonbridging oxygen per tetrahedrally-coordinated cation in individual Q-species.

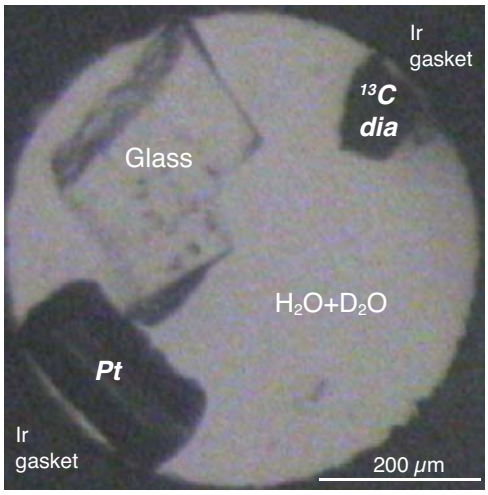

Fig. 1

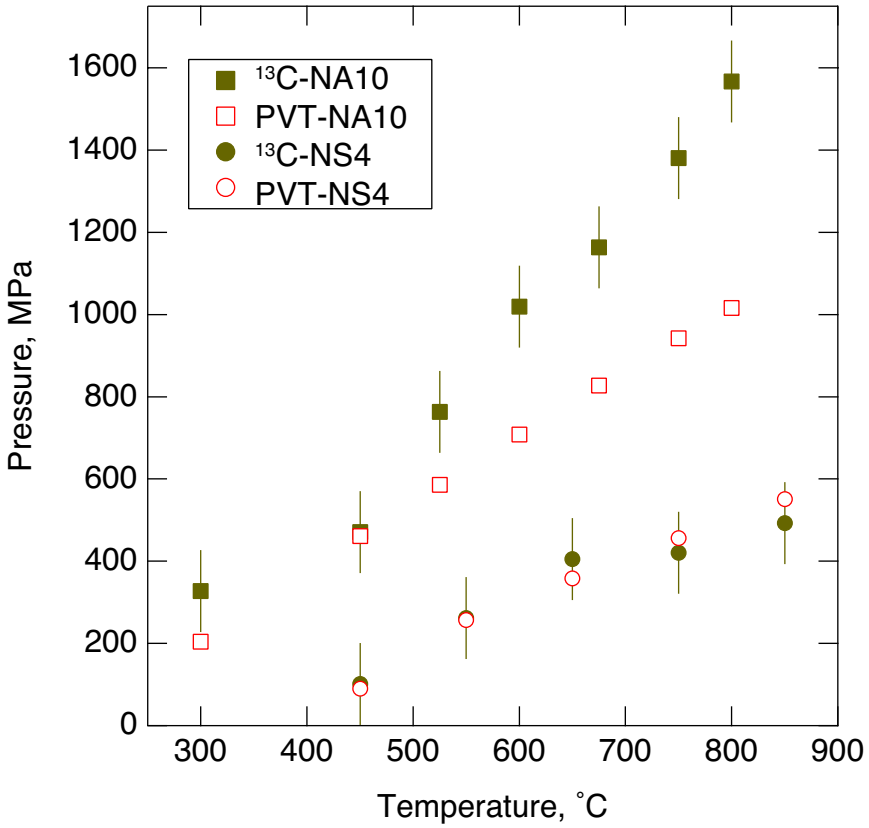
^{13}C-NA10
PVT-NA10
^{13}C-NS4
PVT-NS4
Pressure, MPa
Temperature, ˚C
0
200
400
600
800
1000
1200
1400
1600
300
400
500
600
700
800
900

Fig. 2

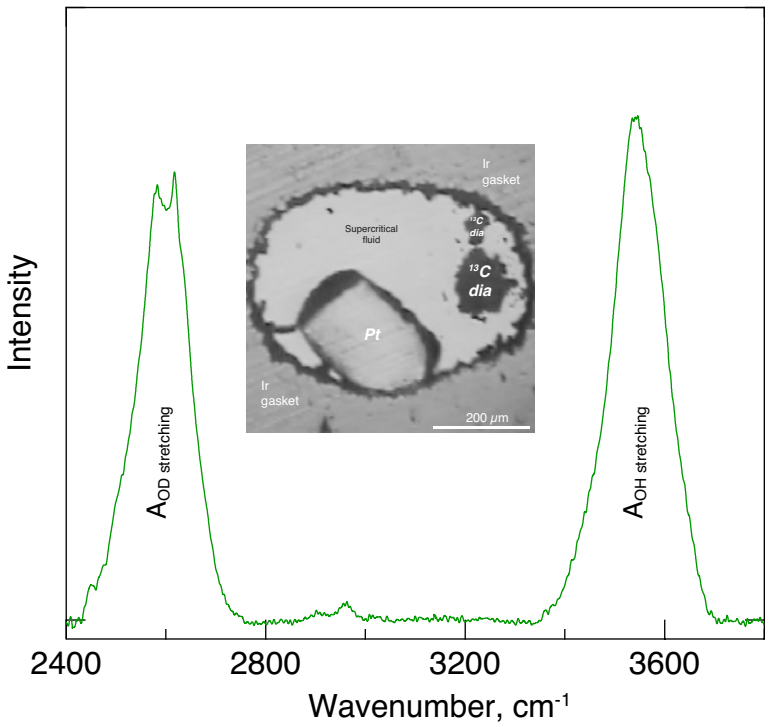
Intensity
Wavenumber, cm-1
2400
2800
3200
3600
AOD stretching
AOH stretching
Ir gasket
Supercritical fluid
13C dia
Pt
Ir gasket
200 μm

Fig. 3

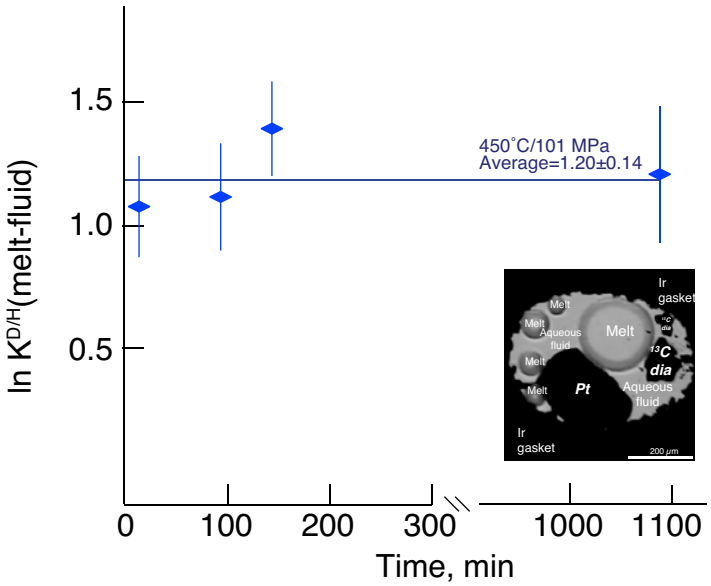
1.5
1.0
0.5
ln K$^{D/H}$(melt-fluid)
450˚C/101 MPa
Average=1.20±0.14
0
100
200
300
1000
1100
Time, min
Ir gasket
Melt
Melt
Aqueous fluid
Melt
Melt
Pt
Melt
^{13}C dia
Aqueous fluid
Ir gasket
200 μm

Fig. 4

This is a preprint, the final version is subject to change, of the American Mineralogist (MSA)
Cite as Authors (Year) Title. American Mineralogist, in press.
(DOI will not work until issue is live.) DOI: http://dx.doi.org/10.2138/am.2013.4247

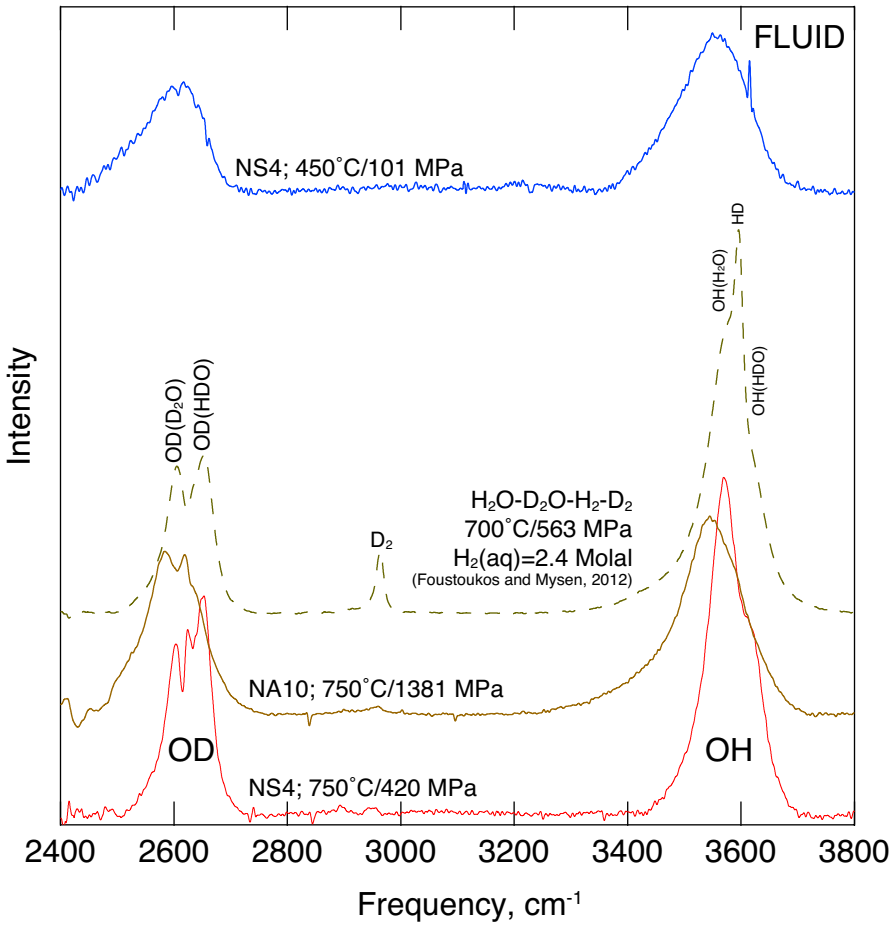

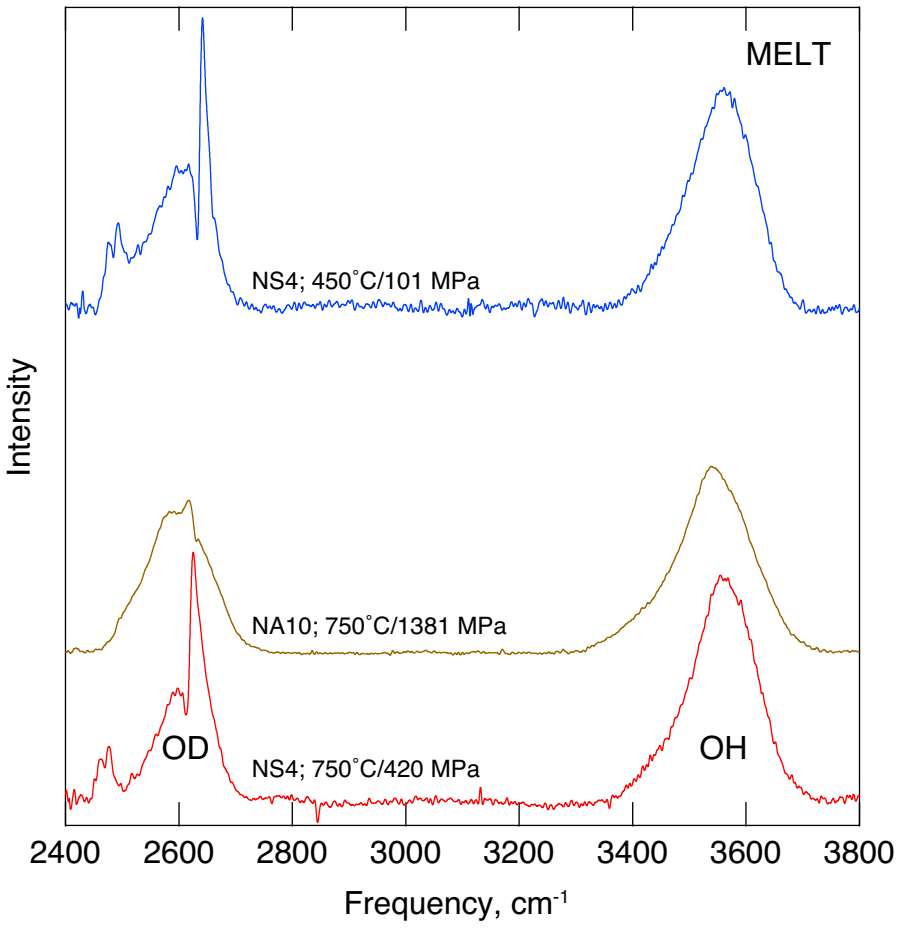

Fig. 5

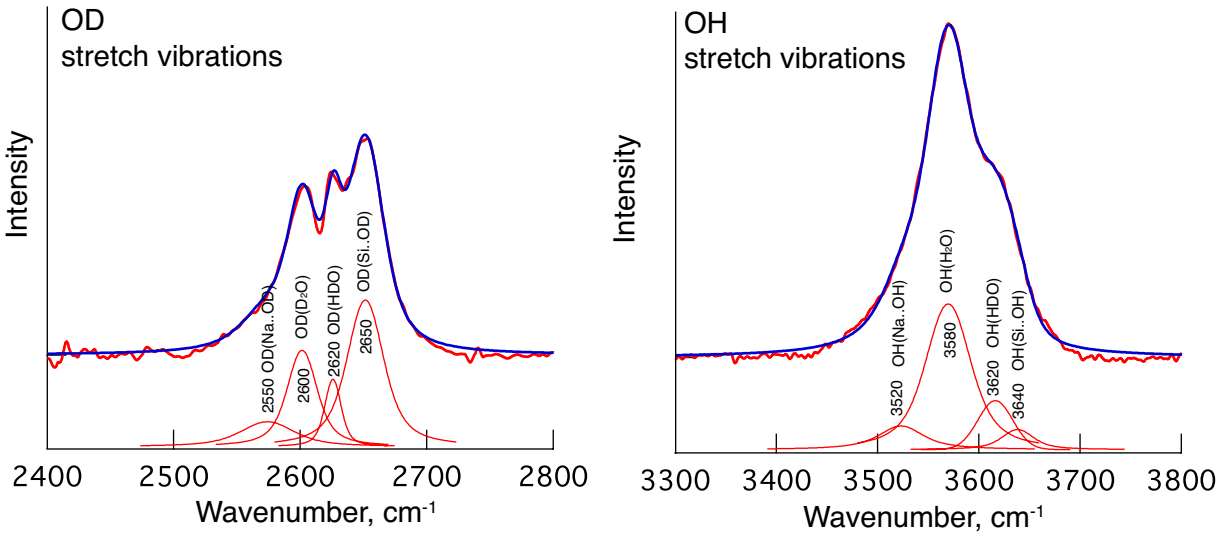
OD
stretch vibrations
Intensity
2550 OD(Na..OD)
2600 OD(D2O)
2620 OD(HDO)
2650 OD(Si..OD)
2400 2500 2600 2700 2800
Wavenumber, cm-1
OH
stretch vibrations
Intensity
3520 OH(Na..OH)
3580 OH(H2O)
3620 OH(HDO)
3640 OH(Si..OH)
3300 3400 3500 3600 3700 3800
Wavenumber, cm-1

Fig. 6

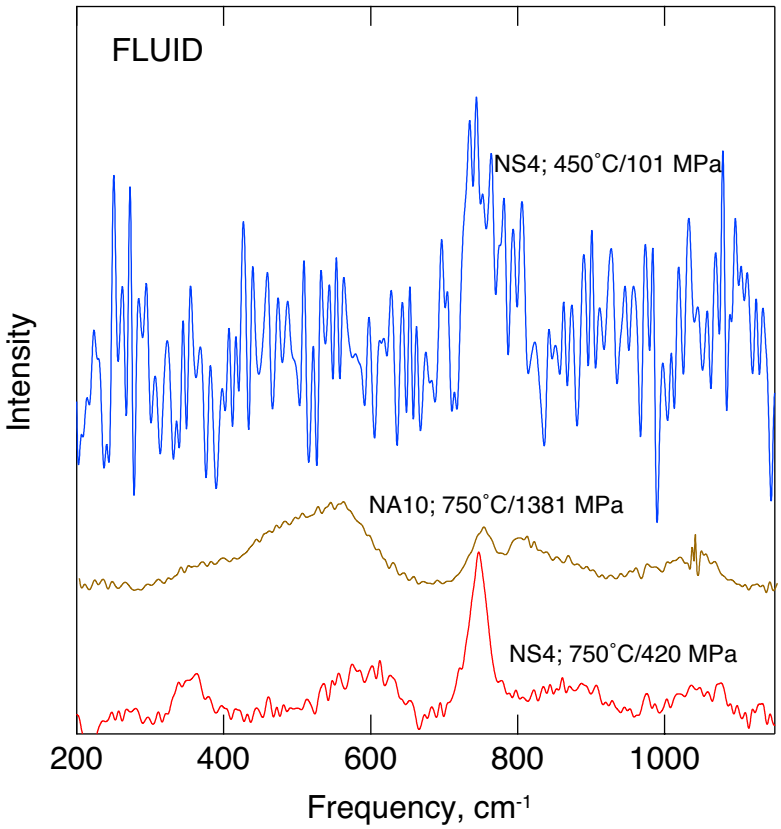
FLUID
NS4; 450˚C/101 MPa
NA10; 750˚C/1381 MPa
NS4; 750˚C/420 MPa
Intensity
200
400
600
800
1000
Frequency, cm-1

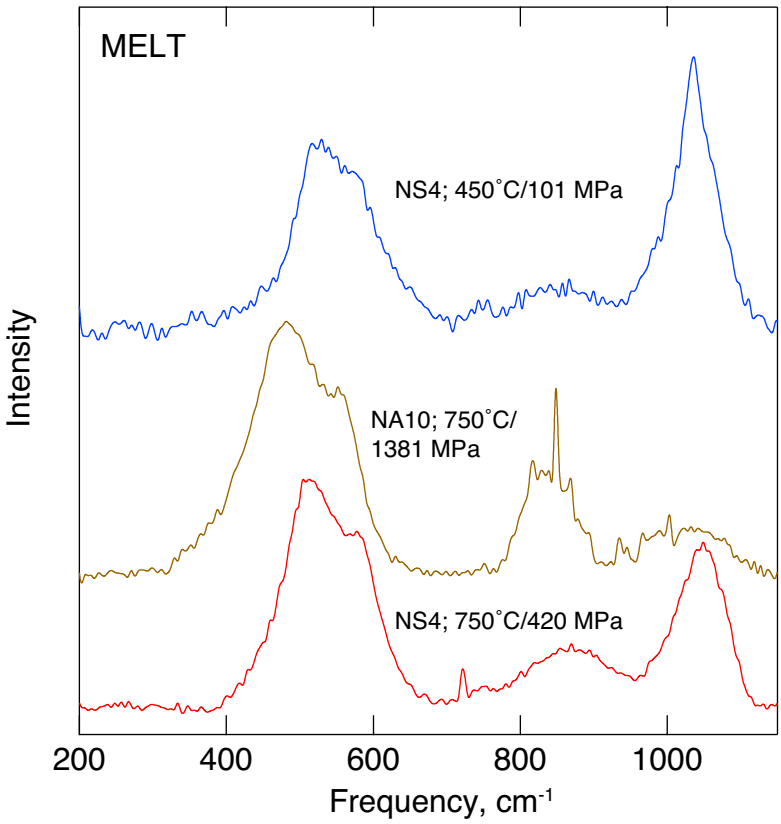
MELT
NS4; 450˚C/101 MPa
NA10; 750˚C/
1381 MPa
NS4; 750˚C/420 MPa
Intensity
200
400
600
800
1000
Frequency, cm-1

Fig. 7

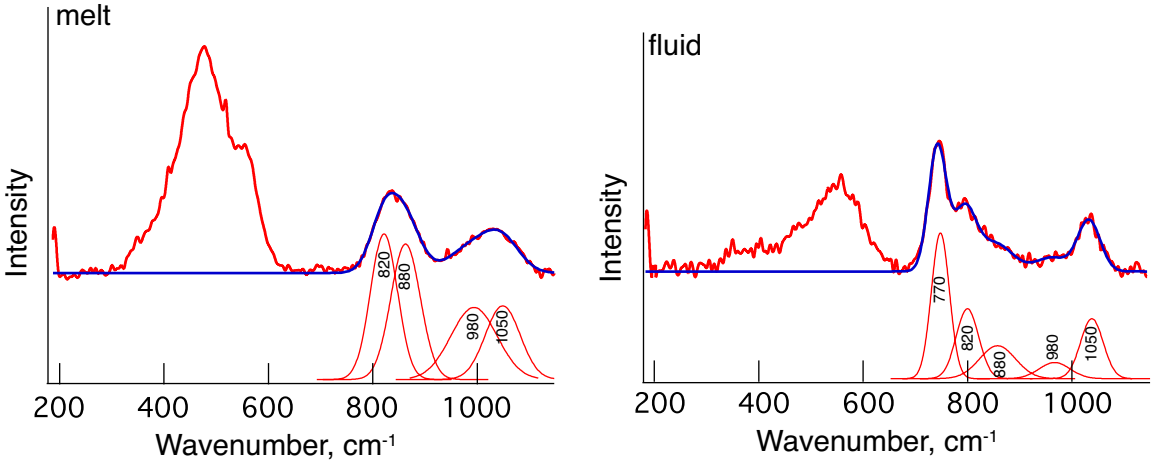
melt
Intensity
820
880
980
1050
200
400
600
800
1000
Wavenumber, cm-1
fluid
Intensity
770
820
880
980
1050
200
400
600
800
1000
Wavenumber, cm-1

Fig. 8

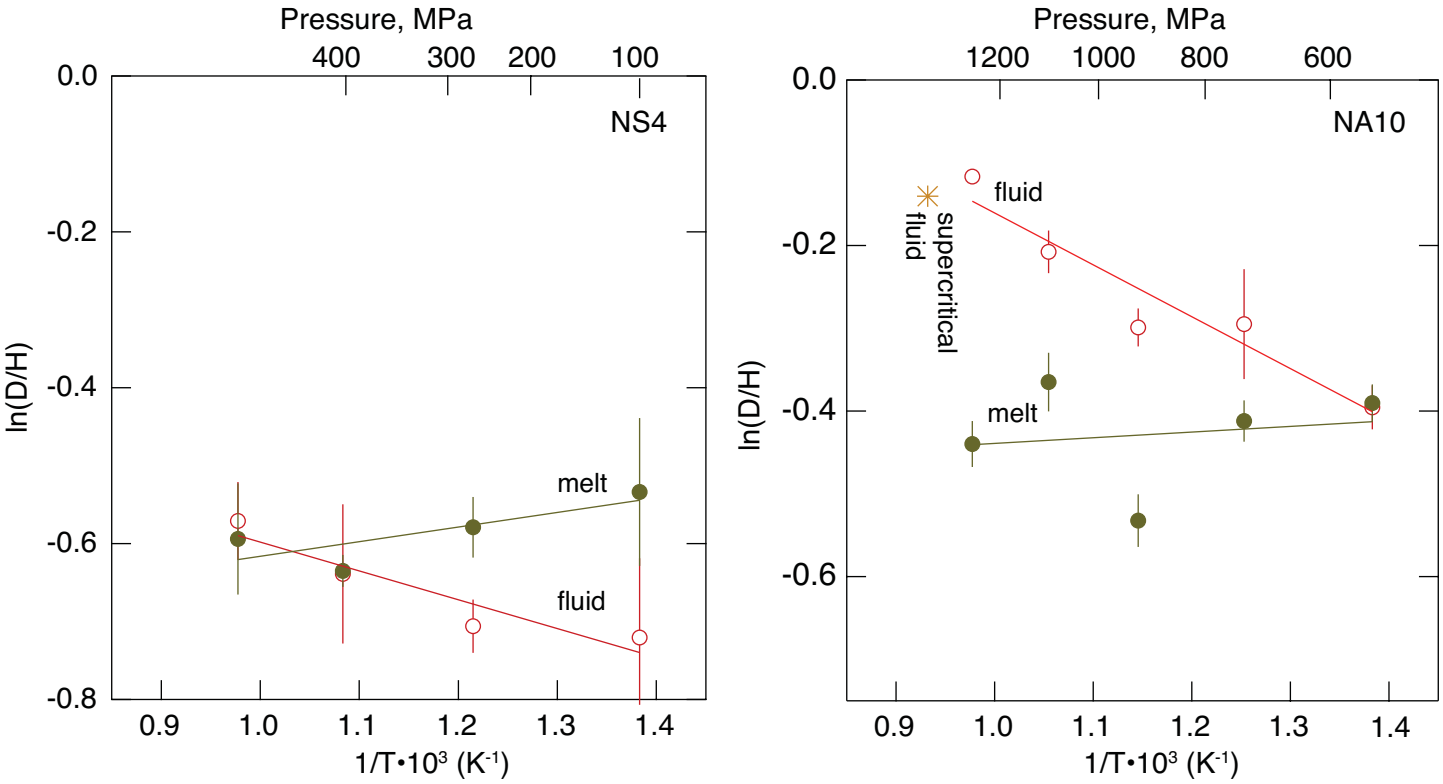
Pressure, MPa
400
300
200
100
NS4
0.0
-0.2
-0.4
-0.6
-0.8
ln(D/H)
melt
fluid
0.9
1.0
1.1
1.2
1.3
1.4
1/T•10³ (K⁻¹)
Pressure, MPa
1200
1000
800
600
NA10
supercritical fluid
fluid
melt

Fig. 9

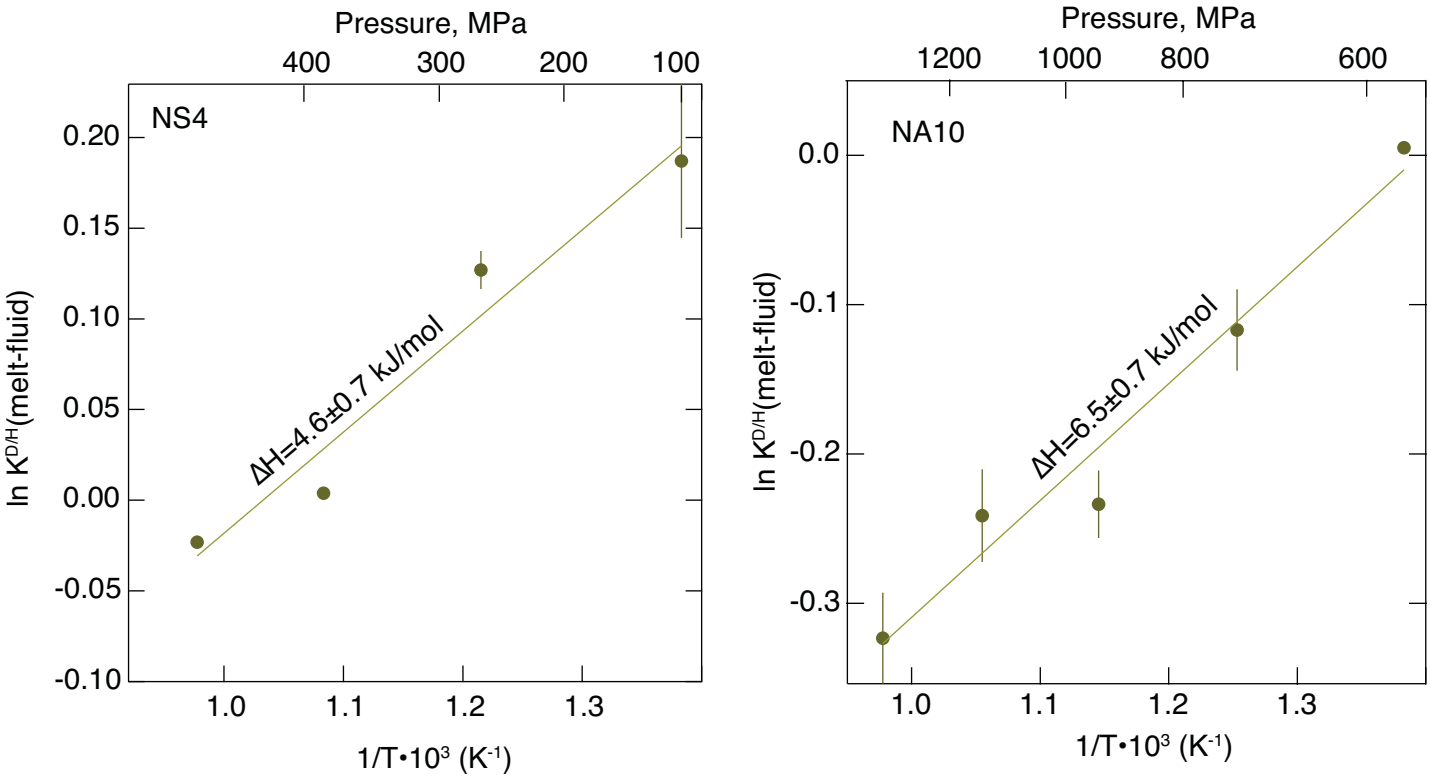
Pressure, MPa
400
300
200
100
NS4
0.20
0.15
0.10
0.05
0.00
-0.05
-0.10
ln K^D/H(melt-fluid)
ΔH=4.6±0.7 kJ/mol
1.0
1.1
1.2
1.3
1/T•10^3 (K^-1)
Pressure, MPa
1200
1000
800
600
NA10
0.0
-0.1
-0.2
-0.3
ln K^D/H(melt-fluid)
ΔH=6.5±0.7 kJ/mol
1.0
1.1
1.2
1.3
1/T•10^3 (K^-1)

Fig. 10

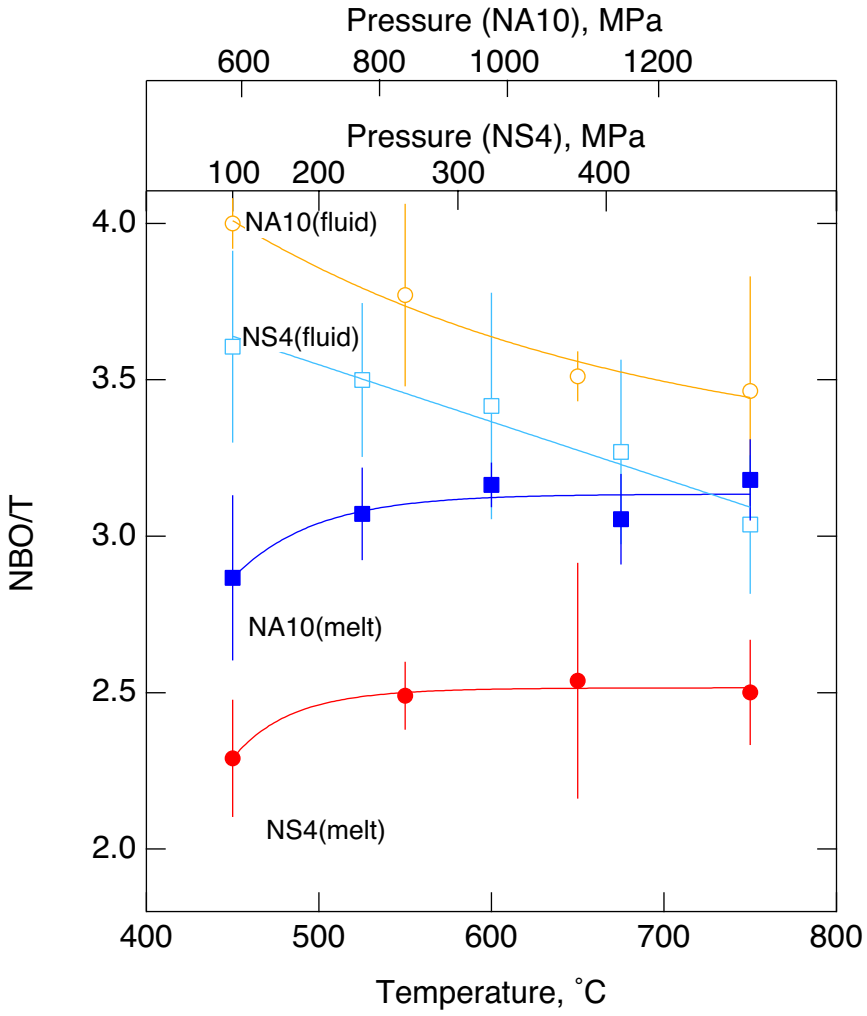
Pressure (NA10), MPa
600
800
1000
1200
Pressure (NS4), MPa
100
200
300
400
NA10(fluid)
NS4(fluid)
NA10(melt)
NS4(melt)
NBO/T
4.0
3.5
3.0
2.5
2.0
400
500
600
700
800
Temperature, ˚C

Fig. 11